Original Article

JCBFM

Journal of Cerebral Blood Flow & Metabolism
2022, Vol. 42(6) 952–965

DOI: 10.1177/0271678X211067133
journals.sagepub.com/home/jcbfm
SAGE

RAGE-mediated T cell metabolic reprogramming shapes T cell inflammatory response after stroke

Yueman Zhang[1,*], Fengshi Li[2,*], Chen Chen[1], Yan Li[1], Wanqing Xie[1], Dan Huang[1], Xiaozhu Zhai[1], Weifeng Yu[1], Jieqing Wan[2] and Peiying Li[1,*]

Abstract

The metabolic reprogramming of peripheral $CD4^+$ T cells that occurs after stroke can lead to imbalanced differentiation of $CD4^+$ T cells, including regulation of T cells, and presents a promising target for poststroke immunotherapy. However, the regulatory mechanism underlying the metabolic reprogramming of peripheral $CD4^+$ T cell remains unknown. In this study, using combined transcription and metabolomics analyses, flow cytometry, and conditional knockout mice, we demonstrate that the receptor for advanced glycation end products (RAGE) can relay the ischemic signal to $CD4^+$ T cells, which underwent acetyl coenzyme A carboxylase 1(ACC1)-dependent metabolic reprogramming after stroke. Furthermore, by administering soluble RAGE (sRAGE) after stroke, we demonstrate that neutralization of RAGE reversed the enhanced fatty acid synthesis of $CD4^+$ T cells and the post-stroke imbalance of Treg/Th17. Finally, we found that post-stroke sRAGE treatment protected against infarct volume and ameliorated functional recovery. In conclusion, sRAGE can serve as a novel immunometabolic modulator that ameliorates ischemic stroke recovery by inhibiting fatty acid synthesis and thus favoring $CD4^+$ T cells polarization toward Treg after cerebral ischemia injury. The above findings provide new insights for the treatment of neuroinflammatory responses after ischemia stroke.

Keywords

Ischemic stroke, RAGE, fatty acid synthesis, T cell differentiation, ACC1

Received 20 August 2021; Revised 26 October 2021; Accepted 26 November 2021

Introduction

Stroke is the leading cause of adult disability and causes 6 million deaths annually around the world.[1] Unfortunately, treatments for ischemic stroke are still limited to thrombolysis and mechanical thrombectomy, thus novel therapeutic targets are desperately needed.[2,3] Immune response is a prominent pathological feature in ischemic stroke; investigations into the post-stroke immune intervention may help in the development of new therapies for ischemic stroke.[4–8]

Regulation T cell function is an emerging field of stroke treatment, with a particular focus on Tregs.[9–13] Previous studies suggest that post-stroke interventions targeting peripheral T cells affect prognostic indicators, with increased attention that metabolism impacts T cell differentiation.[14–16] Berod et al. found that the glycolytic-fatty acid synthesis pathway is an important

[1]Department of Anesthesiology, State Key Laboratory of Oncogenes and Related Genes, Shanghai Cancer Institute, Renji Hospital, Shanghai Jiao Tong University School of Medicine, Shanghai, China
[2]Department of Neurological Surgery, Ren Ji Hospital, Shanghai Jiao Tong University School of Medicine, Shanghai, China

*These authors contributed equally to this work.

Corresponding authors:
Peiying Li, Department of Anesthesiology, State Key Laboratory of Oncogenes and Related Genes, Shanghai Cancer Institute, Renji Hospital, Shanghai Jiao Tong University School of Medicine, Shanghai 200127, China.
Email: peiyingli.md@gmail.com

Jieqing Wan, Department of Neurosurgery, Renji Hospital, Shanghai Jiao Tong University School of Medicine, 160 Pujian Rd, Shanghai 200127, China.
Email: Jieqingwan@126.com

checkpoint that determines the differentiation of naive $CD4^+$ T cells into different effector T cells.[16] We previously reported that the metabolic reprogramming of $CD4^+$ T cells after stroke could modulate the balance of Treg/Th17 and thus affect post-stroke neuroinflammation.[17] However, how the ischemic signals of early brain injury after stroke interface with peripheral $CD4^+$T cells remains largely unexplored.

Ischemic brain tissue can release a number of damage-associated molecular patterns (DAMPs), such as high mobility group box-1 (HMGB1), which activate the Toll-like receptor (TLR) and the receptor for advanced glycation end products (RAGE) on peripheral monocytes.[4,18,19] RAGE is also expressed on T cells and is positively associated with the up-regulation of pro-inflammatory signaling pathways, such as NF-kB activation.[18,20] However, whether the activation of RAGE receptors plays a role in transmitting the danger signal from the ischemic brain to the intracellular metabolic pathway in peripheral naive $CD4^+$ T cells remains unknown.

Our current study describes that the activation of RAGE by the DAMPs signal after ischemic stroke controls fatty acid metabolic reprogramming in $CD4^+$ T cells and thus induces the differentiation of naive $CD4^+$T cells into Th17 instead of Tregs. Administrating soluble RAGE (sRAGE) attenuated ischemic infarct growth and promoted functional recovery after stroke by inhibiting fatty acid synthesis, favoring $CD4^+$ T cells differentiation toward Tregs.

Materials and methods

Animals

Male C57BL/6 mice were purchased from Shanghai SLAC Laboratory Animals and were housed under standard laboratory conditions (22 °C and a 12-hour light-dark cycle with free access to food and water). $ACC1^{fl/fl}$ mice on C57BL/6 background were crossed to CD4-Cre mice to generate $CD4^{cre}ACC1^{fl/fl}$ mice ($CD4^+$ T cells conditioned knockout ACC1).[16] $ACC1^{fl/fl}CD4\text{-}Cre^-$ littermates were used as wild-type (WT) controls in all experiments. Both CD4-Cre mice and $ACC1^{fl/fl}$ mice were gifts from Professor Tim Sparwasser (Hannover, Germany). All experiments were approved by the Renji Hospital Institutional Animal Care and Use Committee and performed in accordance with the Institutional Guide for the Care and Use of Laboratory Animals.

Murine focal ischemia model

Male 8 to 10-week-old wild type, $ACC1^{fl/fl}$ and $CD4^{cre}ACC1^{fl/fl}$ mice on C57BL/6 background were subjected to transient MCAO (MCAO) as previously described.[21] Briefly, mice were anesthetized with 2% isoflurane in a 30% O_2/70%N_2 mixture. A skin incision was made at the neck and the left CCA was exposed and ligated. We induced MCAO by intraluminal occlusion of the left MCA for 1 hour. Sham-operated animals underwent anesthesia and surgical exposure of arteries but without artery occlusion. Body temperature was maintained at 37 ± 0.5 °C with a heating pad during surgical procedures. sRAGE (50 μg per mouse in 200 μl, 1179-RG-050, R&D) was administered by intravenously injection 15 min before MCAO plus 90 min after MCAO (sRAGE).[22]

Randomization, blinding and study timeline

All behavioral procedures, histological and flow cytometry assessments were performed by investigators blinded to experimental group assignments. Randomization were performed using the envelop method. The overall study timeline is as follows:

1. Day 0: MCAO, Day 3: Collect tissue for immunostaining, flow cytometry, RNA sequencing and LC-MS.
2. Day 0: MCAO; Day-1–28: Day -1, 1, 3, 5, 7, 14, 28 for neurological deficit score, adhesive removal and grid walk; Day 30: Collect tissue flow cytometry.

Animals were excluded if the suture was not successfully placed to occlude the MCA which was monitored by two-dimensional laser speckle. Animal data reporting followed The ARRIVE 2.0 guidelines[23]

Two-dimensional laser speckle imaging techniques

Cerebral blood flow (CBF) was monitored by two-dimensional laser speckle technique. Briefly, cerebral perfusion images were acquired using the PeriCam PSI System (Perimed) positioned above the mice head before, during ischemia and after reperfusion. Speckle contrast was defined as the ratio of SD of pixel intensity to the mean pixel intensity. The speckle visibility relative to the velocity of the light-scattering particles was converted to correlation time values, which are inversely and linearly proportional to the mean blood velocity. CBF changes were expressed as a percentage of pre-MCAO baselines.

Transcriptome experimental method and data analysis

Experimental methods. Total RNA was isolated using the Trizol Reagent (Invitrogen Life Technologies), after which the concentration, quality and integrity were

determined using a NanoDrop spectrophotometer (Thermo Scientific). Three micrograms of RNA were used as input material for the RNA sample preparations. Sequencing libraries were generated according to the following steps. Firstly, mRNA was purified from total RNA using poly-T oligo-attached magnetic beads. Fragmentation was carried out using divalent cations under elevated temperature in an Illumina proprietary fragmentation buffer. First strand cDNA was synthesized using random oligonucleotides and Super Script II. Second strand cDNA synthesis was subsequently performed using DNA Polymerase I and RNase H. Remaining overhangs were converted into blunt ends via exonuclease/polymerase activities and the enzymes were removed. After adenylation of the 3′ ends of the DNA fragments, Illumina PE adapter oligonucleotides were ligated to prepare for hybridization. To select cDNA fragments of the preferred 400–500 bp in length, the library fragments were purified using the AMPure XP system (Beckman Coulter, Beverly, CA, USA). DNA fragments with ligated adaptor molecules on both ends were selectively enriched using Illumina PCR Primer Cocktail in a 15 cycle PCR reaction. Products were purified (AMPure XP system) and quantified using the Agilent high sensitivity DNA assay on a Bioanalyzer 2100 system (Agilent). The sequencing library was then sequenced on NovaSeq 6000 platform (Illumina) by AigenX Biosciences Co., Ltd.

Data analysis

Quality control. Samples are sequenced on the platform to get image files, which are transformed by the software of the sequencing platform, and the original data in FASTQ format (Raw Data) is generated. Sequencing data contains a number of connectors, low-quality reads, so we use Cutadapt (v1.15) software to filter the sequencing data to obtain high quality sequences (i.e., clean data) for further analysis.

Reads mapping. The reference genome and gene annotation files were downloaded from genome website. The filtered reads were mapped to the reference genome using HISAT2 v2.0.5.

Differential expression analysis. We used HTSeq (0.9.1) statistics to compare the Read Count values on each gene as the original expression of the gene, and then used FPKM to standardize the expression. The difference between expression of genes was analyzed by DESeq (1.30.0) with screening conditions as follows: expression difference multiple $\log^2$FoldChange >1, significant P-value <0.05. At the same time, We used R language Pheatmap (1.0.8) software package to perform bi-directional clustering analysis of all different genes of samples. Heatmaps were generated according to the expression level of the same gene in different samples and the expression patterns of different genes in the same sample with Euclidean method to calculate the distance and Complete Linkage method to cluster.

GO and KEGG enrichment analysis. We mapped all the genes to Terms in the Gene Ontology (GO) database and calculated the numbers of differentially enriched genes in each Term. Using top GO to perform GO enrichment analysis on the differential genes, we calculated the P-value by hypergeometric distribution method (the standard of significant enrichment is P-value <0.05), and found the GO term with significantly enriched differential genes to determine the main biological functions performed by differential genes. ClusterProfiler (3.4.4) software was used to carry out the enrichment analysis of the KEGG pathway of differential genes, focusing on significant enrichment pathways with P-value <0.05

Interaction analysis of differential gene protein network. The STRING database (https://string-db.org/) was used for protein interaction analysis to reveal the relationship between target genes.

Metabolome experimental methods and data analysis

Experimental methods. Metabolite samples were analyzed via LC-Orbitrap-MS (Thermo Q Exactive coupled with Waters Acquity UPLC). The column was Acquity UPLC BEH C18 (2.1*100 mm 1.7 μm). Mobile phase A contained water with 0.05% methanoic acid, and mobile phase B was 100% acetonitrile. The gradient was as follows: 0 min, 95% A; 1 min, 95% A; 12 min, 5% A; 13.5 min, 5% A; 13.6 min, 95% A; 16 min, 95% A with a flow rate of 0.3 mL/min. The total Ions Chromatographs spectra were acquired in the positive and negative electrospray ionization mode. The capillary of the ESI source was set to 300 °C, with sheath gas at 45 arbitrary units, auxiliary gas at 15 arbitrary units and the spray voltage at 3.0 kV (ESI+) 3.2KV (ESI−). In positive and negative mode, an m/z scan range from 70 to 1050 was chosen and MS1 data were collected at a resolution of 70,000. The automatic gain control (AGC) target was set at 3×10^6 and the maximum injection time was 100 ms. The top ten precursor ions were subsequently fragmented, in a data-dependent manner, using the higher energy collisional dissociation (HCD) in MS2 at a resolution power of 17,500. Sample volumes of 15 μL were injected. Data acquisition and analysis were carried out

by Compound Discoverer 3.1 software (Thermo Fisher Scientific).

Data analysis. The LC-MS/MS data analysis was pre-processed using Compound Discoverer 3.1 software (Thermo Fisher Scientific). Spectra obtained were subjected to multivariate statistical analysis; 1873 and 2490 variables based on metabolic features were obtained either in the positive mode (ESI+) or in the negative mode (ESI−). SIMCA14.1 (Umetrics AB, Umea, Sweden) was used as the statistical software for multivariate and univariate analyses of metabolite data sets from a total of 9 samples consisting of three biological replicates and three different groups. Principle components analysis (PCA), partial least squares discriminant analysis (PLS-DA) and orthogonal partial least square discriminant analysis (OPLS-DA) were applied to obtain the intrinsic variance in data sets. Metabolite differences were evaluated using Student's t-test analysis (with $P < 0.05$) and variable influence on project score (VIP > 1) of OPLS-DA. We analyzed the identified metabolites related pathways based on Kyoto Encyclopedia of Genes and Genomes (KEGG) pathway database.

Measurements of infarct volume

For microtubule-associated protein 2 (MAP-2) staining, animals were sacrificed and perfused transcardially with 0.9% normal saline and 4% paraformaldehyde in PBS. Free-floating sections were prepared from the fixed and dehydrated brains, then stained with a MAP-2 antibody (1:500, abcam). Infarct volume was determined with NIH Image J (1.52a) analysis by an observer "blinded" to the experimental group assignment.

Flow cytometry

For splenocytes and peripheral blood cells, single cell suspensions were prepared using RBC lysis buffer (BD) and filtered through a 70 μm nylon membrane. For brain tissues, we homogenized the hemisphere ipsilateral to the infarct using a Neural Tissue Dissociation Kit (MACS) by the gentle MACS Dissociator following the manufacturer's instructions (Miltenyi Biotec). The immune-cell-enriched population of cells was collected using a Percoll gradient. For intracellular cytokine staining, single-cell suspensions from spleens and blood were stimulated with phorbol myristate acetate (PMA) (50 ng/ml, Fisher BioReagents) and ionomycin (750 ng/ml, Millipore Sigma) in the presence of GolgiStopTM (1:1000, BD Biosciences) for 4 h at 37 °C/5% CO_2. Isolated cells were surfaced stained accordingly with fluorescent-conjugated antibodies against CD4-BV421 (catalog: 562891, BD, USA), CD25- PE-Cy7 (catalog: 25-0251-82, ebioscience, USA), NK1.1-BV510 (catalog: 563096, BD), CD8a-PE (catalog: 140408, Biolegend), CD45-PE (catalog:553081, BD), CD11b-APC (catalog:553312, BD), Ly6G-PE-y7(catalog: 127618, Biolegend), F4/80-BV421 (catalog:123131, Biolegend). For intracellular transcription factor and cytokine staining, cells were further processed using the Foxp3/Transcription Factor Staining Kit (eBioscience) or the BD Cytofix/Cytoperm Staining Kit (BD Biosciences), respectively, and then stained accordingly with fluorescent-conjugated antibodies against RORγ-APC (catalog: 17-6988-82, ebioscience, USA), Foxp3-PE (catalog: 12-5773-82, ebioscience, USA), IL4-APC (catalog: 17-7041-82, ebioscience, USA), IL-17A-APC (catalog: 17-7177-81, ebioscience, USA), IFNγ- PerCP-Cy5.5 (catalog: 45-7311-82, ebioscience, USA). Stained cells were collected with BD Verse (BD Bioscience) and analyzed with FlowJo software (TreeStar).

Neurological function evaluation

The modified Garcia Score,[24] grid walk,[25] and adhesive test[26] were performed as previously described to assess sensorimotor functions before and after surgery by investigators who were blinded to experimental group assignments. The modified Garcia Score is a well-established sensorimotor assessment system consisting of seven individual tests, of which one measures sensory function while four measure motor function. We scored each test from 0 to 3 (maximal score = 15): (a) body proprioception, (b) forelimb walking, (c) limb symmetry, (d) lateral turning, and (e) climbing as described. The grid walk test was performed according to Rogers et al.[25] with slight modifications. In the grid walk test, mice were placed on an elevated steel grid and the foot fault errors (when the animal's forelimb was misplaced and fell through the grid) were recorded as the mice moved. Data are presented as percentage of foot fault errors for the right impaired forelimb relative to the total amount of right forelimb steps. In the adhesive removal test, two pieces of adhesive tape (0.3*0.4 cm^2) were applied with equal pressure on each animal paw. The order of placement of the adhesive (right or left) was alternated between each animal and each session. Then, the mouse was gently placed in a Perspex box, and the seconds to remove each adhesive tape were recorded. Mice were trained daily before surgery and regularly tested after stroke.

Immunofluorescence

Coronal sections were incubated with 10% normal donkey serum for 30 minutes at room temperature in

PBS containing 0.1% Triton X-100 followed by incubation with appropriate primary antibodies overnight at 4 °C in the same buffer. The anti-Iba-1(1:500, Wako), anti-GFAP (1:500, Abcam), and anti-iNOS (1:300, BD Biosciences) primary antibodies were used. After primary antibody incubation, sections were washed four times at room temperature, followed by incubation with appropriate fluorescent-labeled secondary antibodies (1:1000) for 1 hour at room temperature. DAPI was incubated for counterstaining of the nucleus. Sections were then washed with PBS and mounted with water-based mounting medium containing antifading agents. All the confocal images were captured on a laser scanning confocal microscope (Olympus Fluoview FV3000, Olympus). The numbers of target immunopositive cells were quantified by a blinded investigator using NIH Image J (1.52a). Three randomly selected microscopic fields in the cortex on each section were analyzed for each brain by a blinded investigator. The immunopositive cells were presented as the mean percentage of cells per field (iNOS measured at 40X magnification).

Statistical analysis

All statistics were performed using GraphPad Prism v.6 or the implemented statistical tests of the respective R packages. The Kolmogorov-Smirnov normality test was initially performed on all datasets. Results were presented as mean ± SD. Non-normally distributed data are presented as box-and-whisker plots showing the 25th, 50th, and 75th percentiles and the maximum and minimum values. For normally distributed data, comparisons between two groups were conducted by the two-tailed Student's t-test, and comparisons between multiple groups were conducted by one or two-way ANOVA followed by the Bonferroni *post hoc* test. For continuous variables with non-normal distributions, the two-tailed Mann-Whitney U rank sum test was used. Correlation analyses between continuous data with normal distributions were performed using Pearson analyses. A p-value of <0.05 was deemed significant.

Results

Transcriptome and metabolome combined sequencing reveals metabolic alterations in CD4$^+$ T cells from ACC1-deficient mice after stroke

Our previous study found that glycolysis and fatty acid synthesis in peripheral CD4$^+$ T cells increased significantly after stroke, and that targeted knockout of the key enzyme acetyl coenzyme A carboxylase 1(ACC1) required for de novo fatty acid synthesis in T cells could improve the outcome of ischemic brain injury.[17] In order to explore how ACC1 regulates the transcriptional and metabolic profile of CD4$^+$ T cells after stroke, we isolated CD4$^+$ T cells from blood and spleen of CD4^{cre}ACC1$^{fl/fl}$ or ACC1$^{fl/fl}$ mice 3 days after MCAO (Figure 1(a)). We found that 257 genes were differentially expressed: 198 genes were upregulated and 59 were downregulated (Figure 1(b), Supplementary Table 1). KEGG analyses indicated an enrichment in a number of pathways related to both immune function and the biosynthesis of unsaturated fatty acids (Figure 1(c)). Fatty acid synthesis-related genes (Scd1, Cbr4) and fatty acid transport-related genes (Fabp4) were significantly down-regulated following MCAO in CD4^{cre}ACC1$^{fl/fl}$ mice compared to ACC1$^{fl/fl}$ mice (Figure 1(d)). About 132 metabolites of different chemical classes were detected by metabolomics, 40 of which were significantly different between the two groups. We found that unsaturated fatty acids, medium-chain fatty acids (2-octenedioic acid), and long-chain fatty acids (docosadienoate) in CD4$^+$ T cells of CD4^{cre}ACC1$^{fl/fl}$ mice were significantly reduced (Figure 1(e)). Using KEGG analysis, we found that the significantly altered metabolites were enriched in metabolic pathways, such as biosynthesis of unsaturated fatty acids, oxidative phosphorylation, and phenylalanine metabolism pathways (Figure 1(f)).

RAGE relays an ischemic signal to CD4$^+$ T cells and leads to its metabolic reprogramming after stroke

To explore the underlying mechanism by which how stroke influences T cell metabolic reprogramming, we first examined the expression of immune pattern recognition receptor pathways and found that TLR, RIG, NOD receptor pathways were enriched in the CD4$^+$ T cells from CD4^{cre}ACC1$^{fl/fl}$ mice compared to those from ACC1$^{fl/fl}$ mice following MCAO (Figure 2(a)). Next, we examined the expression of different pattern recognition receptors in CD4$^+$ T cells and found that the expression of the receptor for advanced glycation end products (RAGE) were significantly increased in CD4$^+$ T cells in the blood and spleen from CD4^{cre}ACC1$^{fl/fl}$ mice following stroke, while the expression of toll-like receptor (TLR)1 and TLR2 expression remained unchanged (Figure 2(b) to (i)). TLR4 increased in CD4$^+$ T cells in the spleen of CD4^{cre}ACC1$^{fl/fl}$ mice but did not increase in blood (Figure 2(c) to (i)). The above data suggest that RAGE may relay the ischemic signal to CD4$^+$T cells and lead to ACC1-mediated metabolic reprogramming after stroke.

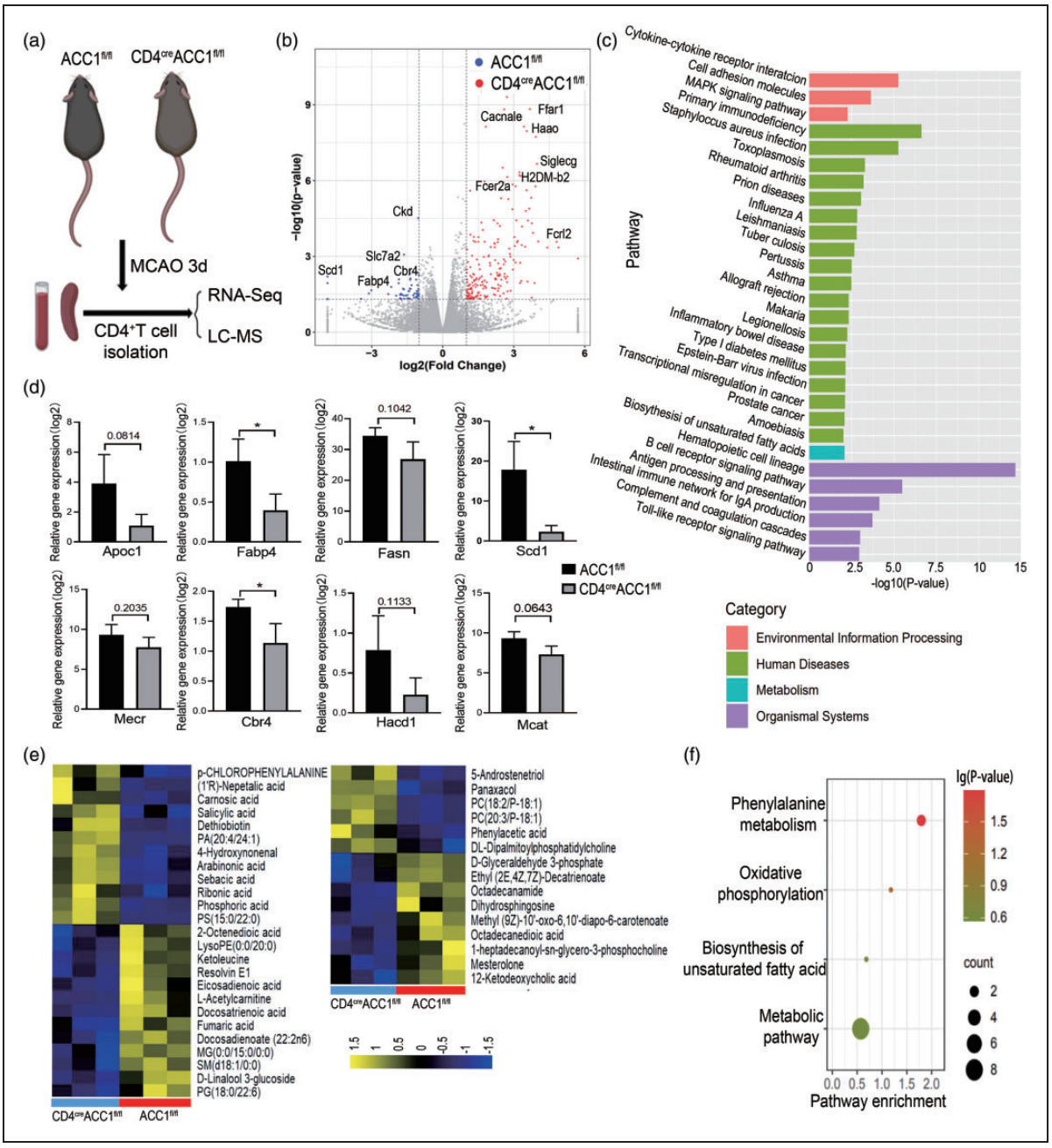

Figure 1. Transcriptic-metabolic jointomics analysis of peripheral CD4$^+$ T cells from CD4^{cre}ACC1$^{fl/fl}$ mice stroke mice. A: Schematic representation of the experimental design. B: Differentially expressed genes (DEGs) displayed on a volcano plot. Red and blue spots represent genes whose expression was significantly changed between the CD4$^+$ T cells from CD4^{cre}ACC1$^{fl/fl}$ and ACC1$^{fl/fl}$ mice after MCAO. Gray spots represent genes without significant changes. C: KEGG pathway enrichment analysis results for all DEGs. D: Relative gene expression of fatty acid metabolism related enzymes. E: Different metabolites were detected in metabolomics between the CD4$^+$ T cells from CD4^{cre}ACC1$^{fl/fl}$ and ACC1$^{fl/fl}$ mice after MCAO. F: KEGG analysis of the significantly altered the metabolites. MCAO: middle cerebral artery occlusion; ACC1: acetyl coenzyme A carboxylase 1; DEG: differentially expressed gene; KEGG: Kyoto Encyclopedia of Genes and Genomes.

Neutralization of RAGE reverses the metabolic reprogramming of CD4$^+$ T cells after stroke

Next, we examined whether blockade of RAGE could reverse the metabolic reprogramming of CD4$^+$ T cells after stroke. First, using metabolomics of peripheral CD4$^+$ cells of mice treated with PBS or sRAGE (RAGE neutralization) by intraperitoneal injection 15 min before MCAO plus 90 min after MCAO, we found that long-chain fatty acids and their derivatives

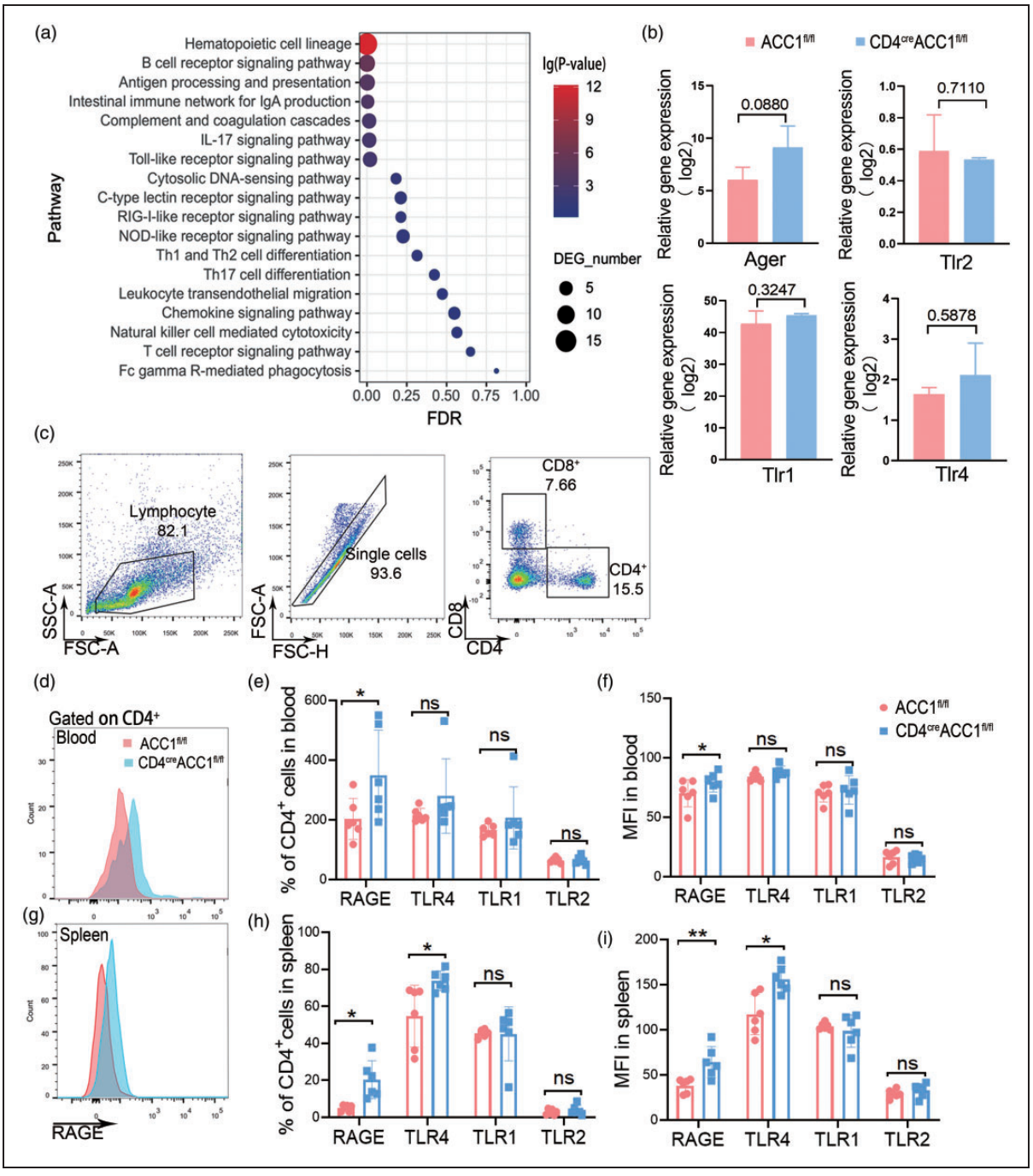

Figure 2. RAGE relays the ischemic signal and leads to metabolic reprogramming of $CD4^+$ T cells. A: KEGG pathway enrichment analysis of immune pathway between the $CD4^+$ T cells from $CD4^{cre}ACC1^{fl/fl}$ and $ACC1^{fl/fl}$ mice after MCAO. B: Relative gene expression of different pattern recognition receptors. C: Representative dot plots and gating strategy for $CD4^+$ T cells sorting followed by flow cytometry. D-I: Representative and quantification of flow cytometry expression of RAGE, TLR1, TLR2, and TLR4 on $CD4^+$ T cells from $CD4^{cre}ACC1^{fl/fl}$ and $ACC1^{fl/fl}$ mice after MCAO. RAGE MFI of $CD4^+$ T cell after MCAO (D, G). Quantification of flow cytometry expression of RAGE, TLR1, TLR2, and TLR4 from $CD4^+$T cells from blood and spleen of $CD4^{cre}ACC1^{fl/fl}$ and $ACC1^{fl/fl}$ mice after MCAO. n = 6 per group. RAGE, the receptor for advanced glycation end products; TLR, Toll-like receptor; FSC, forward scatter; MFI, mean fluorescence intensity; SSC, side scatter. Data are expressed as mean ± SD. *$P \leq 0.05$ and **$P \leq 0.01$. One-way ANOVA, Bonferroni post hoc test.

decreased significantly in sRAGE-treated mice 3 days after stroke (Figure 3(a)). Metabolism (Figure 3(b)) and KEGG (Figure 3(c)) analyses revealed that several metabolic pathways were significantly enriched in $CD4^+$ T cells from sRAGE-treated ischemic mice compared to PBS-treated ischemic mice. In particular, glycerophospholipid metabolism and fatty acid synthesis and decomposition pathways were notably enriched (Figure 3(b) and (c)). To further confirm the transcriptional impact of RAGE neutralization on $CD4^+$ T cells, we explored the expression of fatty acid synthesis-related enzymes, such as ACC1 and Fatty Acid Binding Protein 5 (FABP5), in $CD4^+$ T cells from blood and spleen via flow cytometry. Interestingly, both ACC1 and FABP5 were significantly increased after stroke, but administration of sRAGE attenuated ACC1 and FABP5 expression (Figure 3(c) to (g)). We also examined the lipid droplets and found it decresed in in the blood of sRAGE-treated mice compared to PBS- treated stroke mice (Figure 3(h) to (j)). These data indicate that neutralization of RAGE reverses the metabolic reprogramming of $CD4^+$ T cells after stroke.

Neutralization of RAGE on $CD4^+$ T cells tips the balance of Treg/Th17 cells in the periphery after cerebral stroke

The above data suggest that RAGE may underpin the metabolic reprogramming signal in $CD4^+$ T cells after ischemic stroke. Metabolic reprogramming has been shown to be a robust regulator of $CD4^+$ T cell

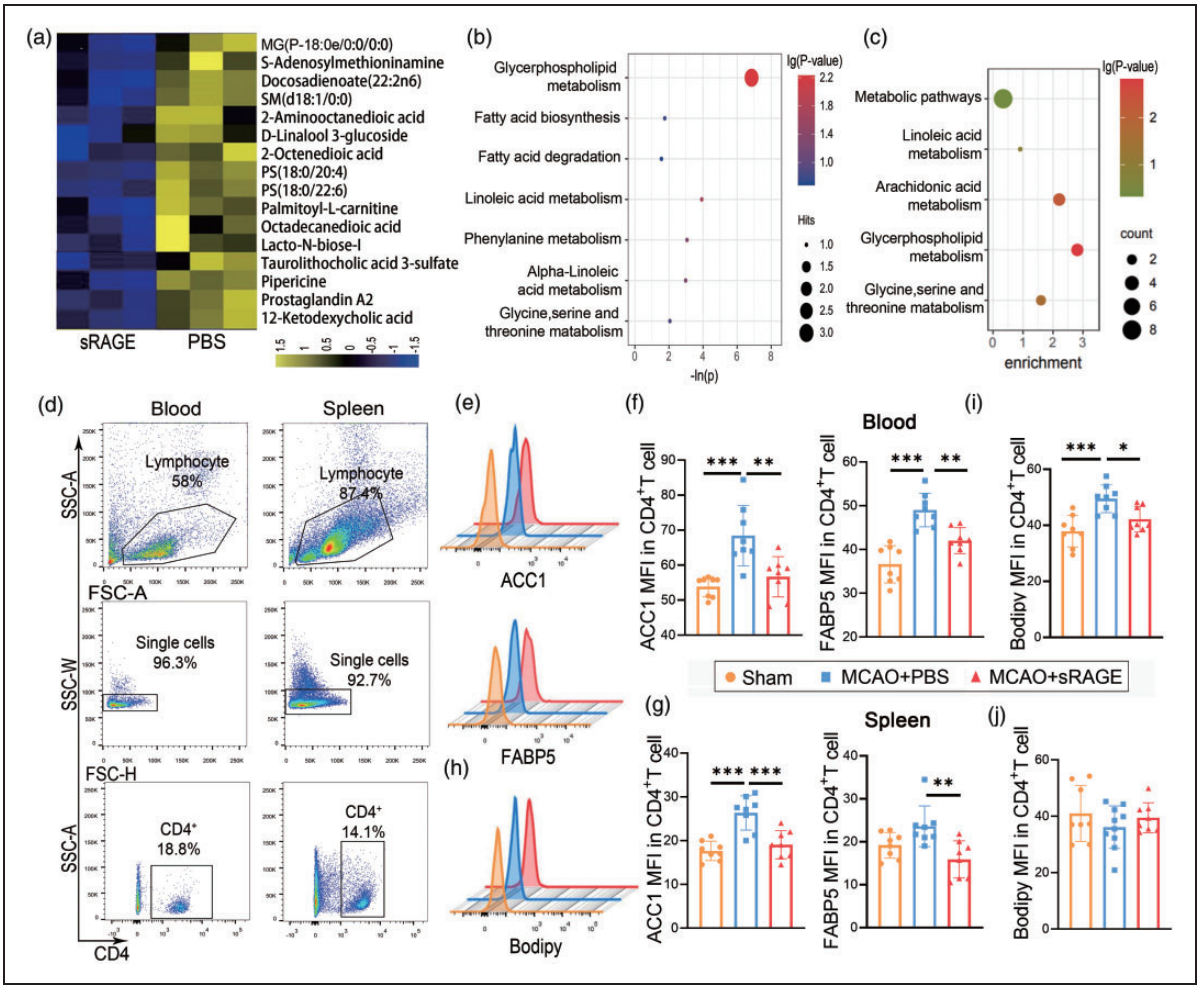

Figure 3. Neutralization of RAGE reverses the metabolic reprogramming of $CD4^+$ T cells after stroke. A: Different metabolites of peripheral $CD4^+$ T cells were detected in metabolomics in sRAGE-treated and PBS-treated mice after MCAO. B: Metabolic analysis of the significantly altered metabolites. C: KEGG analysis of the significantly altered metabolites. D: Representative dot plots and gating strategy for $CD4^+$ T cells sorting followed by flow cytometry. E: Representative image of flow cytometry for ACC1 and FABP5 on $CD4^+$ T cells. F-G: Quantification of mean fluorescent intensity (MFI) of labeled ACC1 and FABP5 on $CD4^+$T cells from blood (F) and spleen (G). H-J: Representative image and quantification of Bodipy flow cytometry on $CD4^+$T cells from blood (I) and spleen (J). $n = 8$ per group. Data are expressed as mean±SD. *$P \leq 0.05$. One-way ANOVA, Bonferroni post hoc test.

differentiation.[27] Thus, we examined whether neutralization of RAGE modulates $CD4^+$ T cell differentiation. We first evaluated the effect of sRAGE treatment on the total number of $CD4^+$ T cells and found administration of sRAGE could lead to a slight increase of the peripheral $CD4^+$ T cells after stroke, but the difference did not reach statistical significance (Figure 4(a) and (b)). Next, we found that the proportion of $CD4^+ROR\text{-}\gamma^+$ T cells (Th17 cells) were significantly decreased, whereas the $CD4^+CD25^+$ $Foxp3^+$cells (Tregs) and the proportion of Treg/Th17 were increased in sRAGE-treated mice compared with WT mice 3 days after MCAO (Figure 4(c) to (f)). In contrast, no significant differences were found in the proportion of $CD4^+IFN\text{-}\gamma^+$ T cells (Th1 cells)/ $CD4^+IL4^+$ T cells (Th2 cells) between the spleens/ blood from sRAGE-treated or PBS- treated stroke mice, although $CD4^+$ $IFN\text{-}\gamma^+$ T cells in the spleen of sRAGE-treated mice were increased compared to PBS-treated stroke mice (Figure S1(a) to (d)). Considering the important role of ACC1 for RAGE pathway mediated metabolic reprogramming, we also administrated sRAGE in $CD4^{cre}ACC1^{fl/fl}$ mice and found there was no difference of Tregs/Th17 cells and Th1/Th2 cells between blood/spleen from the sRAGE-treated $CD4^{cre}ACC1^{fl/fl}$ mice and PBS-treated $CD4^{cre}ACC1^{fl/fl}$ mice 3 days after MCAO (Figure 4(g) to (h), Figure S1(e)). Next, we examined the effect of neutralization of RAGE on T cell differentiation in vitro. In line with our *in vivo* data, the percentage of Treg cells was significantly increased while that of Th17 was decreased in sRAGE-treated cells (Figure S2). We also examined the other immune cells such as neutrophils, macrophages and NK cells, which are known to express RAGE in the spleen and blood and found no difference between the sRAGE-treated or PBS treated mice 3 days after MCAO (Figure S3). These data suggest that neutralization of RAGE in $CD4^+$ T cells reverses the disturbed balance of Tregs/Th17 cells in the periphery after cerebral ischemic stroke.

RNA-sequencing of peripheral $CD4^+$ cells suggests RAGE-dependent interferon signaling in $CD4^+$T cells

To further explore the mechanism that underlies the reversed balance of Tregs/Th17 after neutralizing RAGE, we performed RNA-sequencing on $CD4^+$ T cells from sRAGE-treated and PBS-treated mice 3 days after MCAO. First, we analyzed differential gene expression in $CD4^+$ T Cells from sRAGE-treated and PBS-treated mice 3 days after MCAO and found most of downregulated genes in sRAGE-treated mice were related to the interferon signaling pathway (Figure S4(a)). Using gene ontology (GO) analysis of differential gene expression, an enrichment in type I interferon signaling pathways was observed, which neutralize virus interference and the immune defense (Figure S4(b)). Consistent with the GO pathway analysis, protein-protein interaction (PPI) showed Irf7, a core regulator of interferon signaling pathways, was downregulated in the $CD4^+$ T cells from sRAGE-treated mice after MCAO (Figure S4(c)). As expected, administration of sRAGE also down-regulated fatty acid related genes, such as Cbr4 and Fasn (Figure S4 (d)). Taken together, the interferon signaling pathway and Irf7 may be involved in the RAGE-mediated T cell differentiation and metabolic reprogramming after ischemic stroke.

Treatment of sRAGE reduces infarct volume and neuroinflammation after stroke

Previous studies have suggested that the metabolic reprogramming and differentiation of $CD4^+$ T cells plays an important role in the ischemic brain injury.[17] Therefore, we next examined whether sRAGE treatment could affect the ischemic brain injury after stroke. We administered sRAGE intravenously into MCAO mice 1.5 hours after reperfusion and found the extent of cerebral blood flow reduction was equivalent between the two groups (Figure 5(a) and (b)). Next, we compared infarct volume, measured by MAP2 immunohistochemistry. sRAGE treatment significantly reduced the infarct volume after MCAO (Figure 5(c) and (d)). We also examined BBB disruption by quantifying the extravasation of plasma-derived IgG, and found that sRAGE treatment significantly reduced the BBB disruption in stroke mice. We next investigated the role of sRAGE treatment on poststroke neuroinflammation by measuring astrogliosis and the activation of resident microglia. Consistent with the lesion size, sRAGE decreased the presence of $GFAP^+$ astrocytes and $Iba1^+$ microglia in the ischemic penumbra (Figure S5). Moreover, in the ischemic brain, $CD4^+$ T cells were decreased in sRAGE-treated mice compared to PBS- treated stroke mice, and the proportion of Treg/Th17 in brain were increased in sRAGE-treated mice compared with WT mice 3 days after MCAO (Figure 5(f) to (g)). The above results suggest that sRAGE treatment reduces infarct volume and inhibits neuroinflammatory response in the ischemic brain after stroke.

sRAGE improves long-term functional recovery of MCAO mice

Finally, we also examined the effect of sRAGE on the long-term functional recovery after MCAO using three different behavioral tests, including modified Garcia score, grid-walking test, and adhesive removal test.

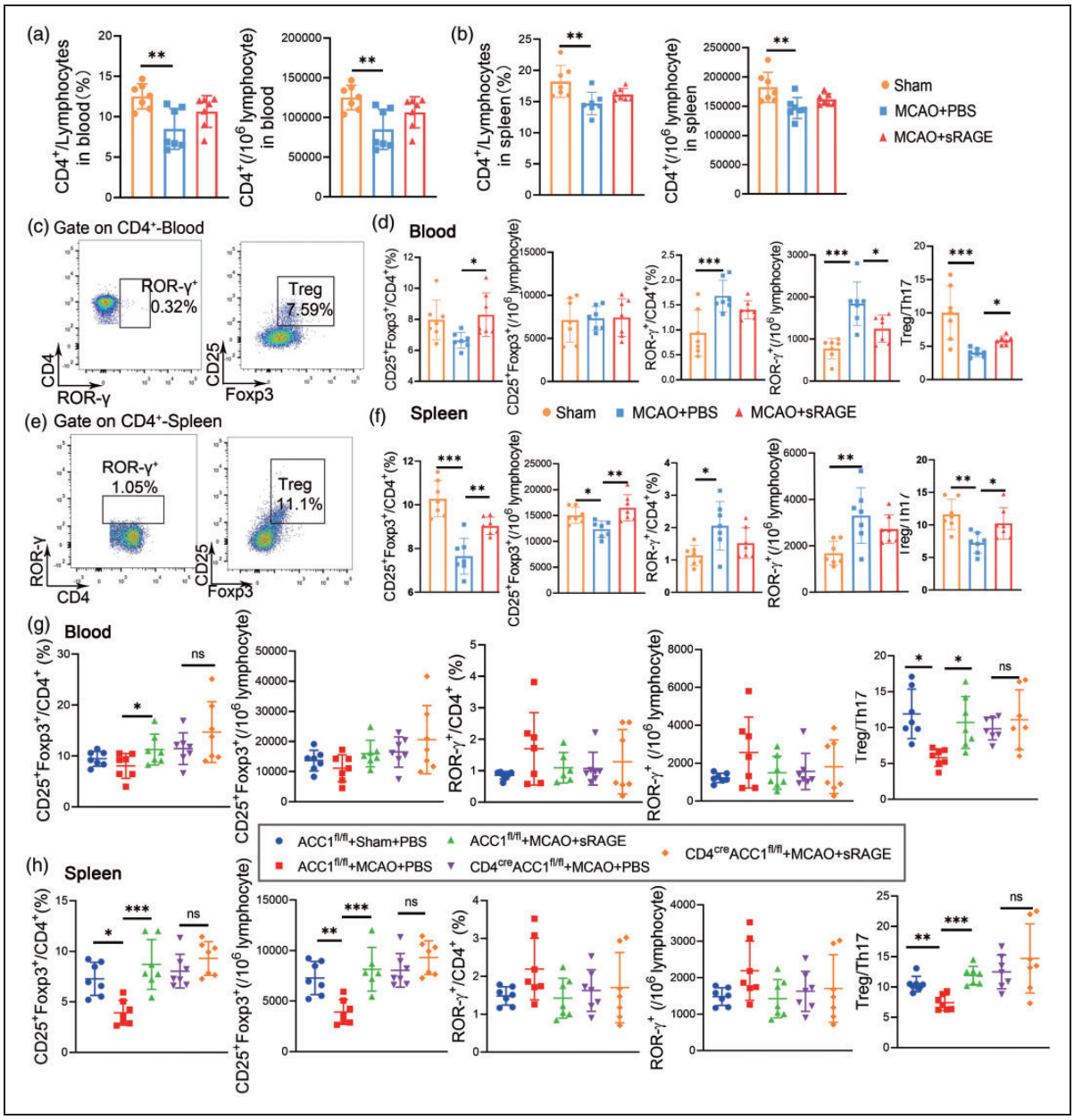

Figure 4. Neutralization of RAGE on $CD4^+$ T Cells tips the balance of Treg/Th17 Cells in the periphery after MCAO. A-B: Quantitative analysis of $CD4^+$ from the blood and spleen of mice from different groups (Sham, PBS+MCAO, sRAGE+MCAO). C-F: Representative flow cytometric plots and quantitative analysis of $CD4^+$ROR-γ^+, and $CD25^+Foxp3^+CD4^+$ T cells from the blood and spleen of mice from different groups (Sham, PBS + MCAO, sRAGE + MCAO). G-H: Representative flow cytometric plots and quantitative analysis of $CD4^+$ROR-γ^+, and $CD25^+Foxp3^+CD4^+$ T cells from the blood and spleen of mice from different groups ($ACC1^{fl/fl}$ + Sham + PBS, $ACC1^{fl/fl}$ + MCAO + PBS, $ACC1^{fl/fl}$ + MCAO + sRAGE, $CD4^{cre}ACC1^{fl/fl}$ + MCAO + PBS, $CD4^{cre}ACC1^{fl/fl}$ + MCAO + sRAGE). n = 7 per group. Data are expressed as mean ± SD. $P > 0.05$, $^*P \leq 0.01$, $^{***}P \leq 0.001$. One-way ANOVA, Bonferroni post hoc test.

sRAGE-treated mice exhibited significantly higher scores in body proprioception, lateral turning and total score compared to the vehicle-treated mice up to 28 days after stroke (Figure 6(a)). In the adhesive removal test, sRAGE-treated mice required shorter time to contact and remove the stickers placed on their paws compared to PBS-treated control mice at 14, 21, and 28 days after stroke (Figure 6(b)). In the grid-walking test, sRAGE-treated mice also made fewer total foot faults at 5 days after stroke (Figure 6 (c)). We also explored whether acute sRAGE treatment exhibits long-term influence on $CD4^+$ T cells

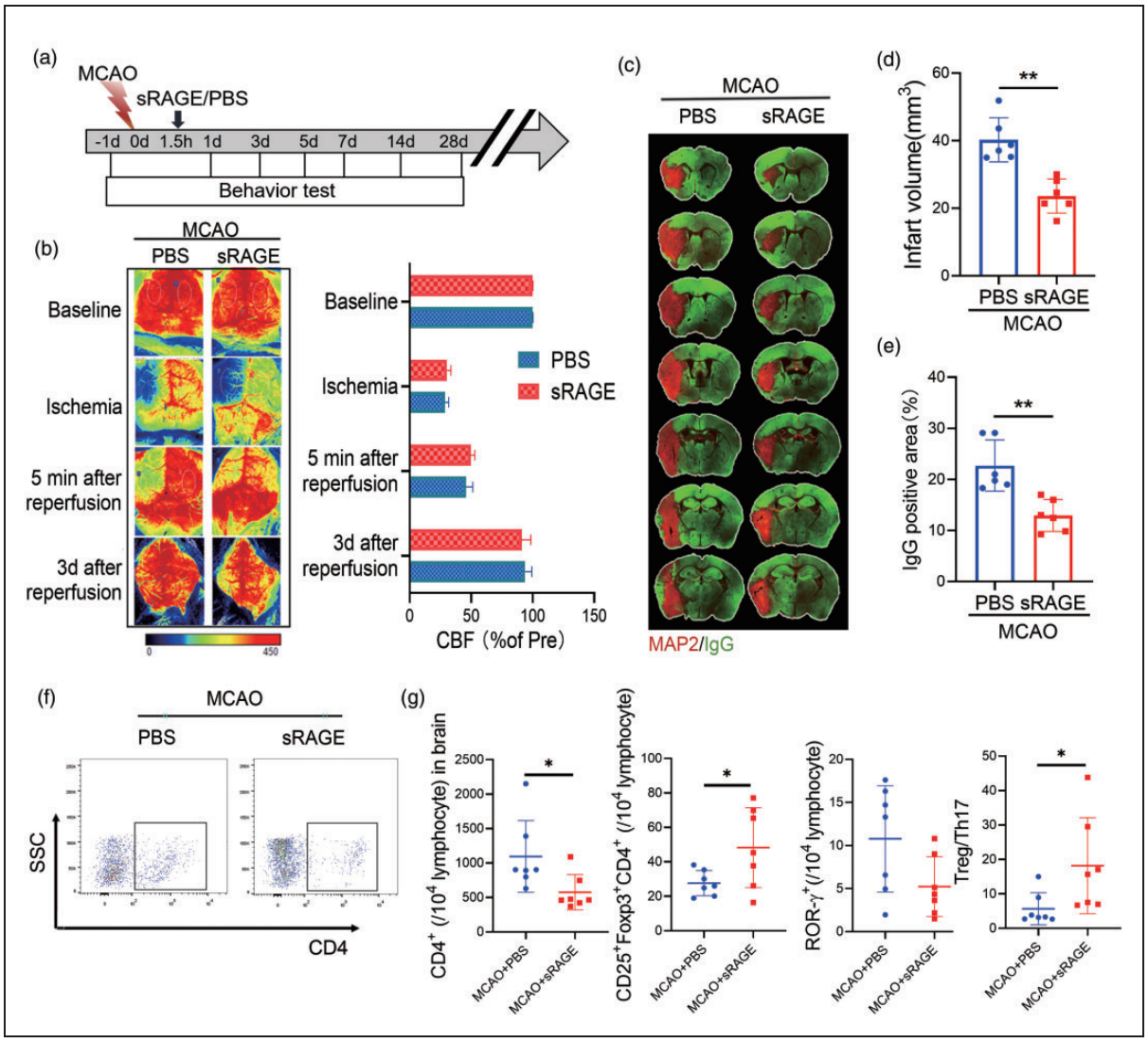

Figure 5. Neutralization of RAGE reduces infarct volume after stroke. (A) Schematic representation of the experimental design. (B) Cerebral blood flow monitored using 2-dimensional laser speckle imaging techniques before, during middle cerebral artery occlusion (MCAO), 5 min and 3 d after reperfusion. Results were expressed as percent change from baseline (pre-MCAO). C: Representative MAP2 staining of brain infarct and endogenous mouse IgG staining of BBB leakage 3 day after stroke in mice treated with sRAGE or PBS. n = 6 per group. D: Quantification of infarct volume 3 day after stroke in mice treated with sRAGE or PBS was determined by immunostaining of in the parenchyma. E: Quantification of endogenous IgG positive area. n = 6 per group. A two-tailed Student's t-test. F-G: Representative flow cytometric plots (F) and quantitative analysis of $CD4^+$, $CD25^+Foxp3^+CD4^+$, $CD4^+ROR\text{-}\gamma^+$ T cells (B) and Treg/Th17 radio (G) from the brain of sRAGE/PBS-treated mice 3 days after MCAO. n = 7 per group. Data are expressed as mean ± SD. $P > 0.05$, $^*P \leq 0.01$, $^{***}P \leq 0.001$. One-way ANOVA, Bonferroni post hoc test.

differentiation after stroke, and found no significant differences in the balance of Treg/Th17 was observed in blood, spleen and brain (Figure S6). Collectively, these results support the concept that posttreatment of sRAGE improves long-term recovery of sensorimotor function after MCAO.

Discussion

This study demonstrates that RAGE, a receptor for DAMPs, mediates the regulation of metabolic reprogramming in peripheral $CD4^+$ T cells after stroke, thereby affecting the differentiation direction of naive $CD4^+$ T cells into Th17/Treg cells. Mechanistically, we revealed that RAGE directs the reprogramming of fatty acid metabolism, which influences the differentiation of $CD4^+$ T cells after cerebral ischemia injury. The above findings could pave the way for the development of immune-adjuvant therapy after stroke.

Cerebral ischemic stroke elicits profound changes in the peripheral immune system, including the early

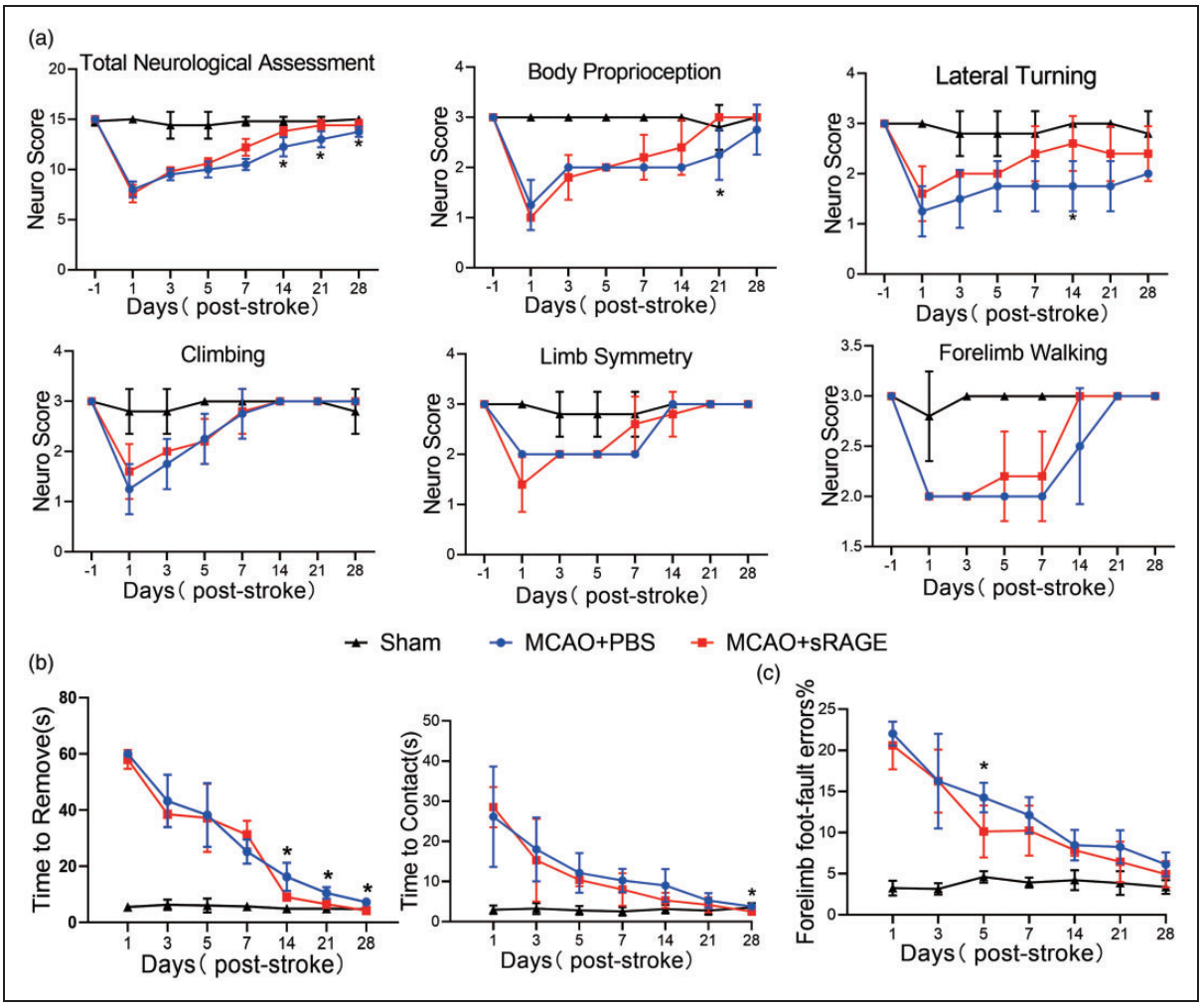

Figure 6. Neutralization of RAGE improves long-term functional recovery of MCAO mice. A-C: Sensorimotor dysfunction was significantly attenuated in sRAGE-treated mice after MCAO, as assessed by the Garcia Score (A), adhesive removal (B) and grid walk (C) test. A: sRAGE-treated mice demonstrated improved scores in body proprioception, lateral turning, and total assessment. B–C: Less sensorimotor deficits were observed in the sRAGE group as reflected by shorter contact and removal time of the sticker and less forelimb foot fault. Data are expressed as mean±SD. *P $\leq$ 0.05, vs PBS. Two-way repeated measures ANOVA for differences between groups. n = 9–10 per group.

immune activation and subsequent immune suppression.[28–31] Our previous study found that peripheral $CD4^+$ T cells underwent metabolic reprogramming with increased glycolysis and fatty acid synthesis after stroke.[17] However, the mechanisms underlying the metabolic reprogramming the $CD4^+$ T cells after stroke remains largely unknown. To explore the regulatory mechanism of metabolic reprogramming of peripheral $CD4^+$ T cells after stroke, we first demonstrated that $CD4^+$ T cells in $CD4^{cre}ACC1^{fl/fl}$ mice did reverse the changes in fatty acid metabolism induced by stroke (Figure 1). Next, using an established transgenic model, we further studied the regulatory mechanism of metabolic reprogramming of peripheral $CD4^+$ T cells after stroke. We found that RAGE receptor was upregulated in peripheral $CD4^+$ T cells of $CD4^{cre}ACC1^{fl/fl}$ mice (Figure 2), which could be a compensatory endogenous mechanism. By neutralization of the RAGE signaling, we found the stroke-induced enhancement of fatty acid synthesis in peripheral $CD4^+$ T cells was reversed (Figure 3), suggesting RAGE could serve as a receptor to relay the brain ischemic signal to the metabolic reprograming of peripheral $CD4^+$T cells. This is the first study that explores the link between brain ischemia damage signals and the metabolic reprogramming of peripheral $CD4^+$ T cells. It was previously suggested that the autonomic nervous system played a significant role in mediating immune regulation after acute brain injury.[32] Liesz et al.[19] suggested that alarmin-mediated pathways and the poststroke stress-related catecholaminergic effects were largely independent in

mononuclear macrophage system. However, the regulation of metabolic reprogramming in peripheral $CD4^+$T cells after stroke remains largely unknown.

In addition to connecting T cell energy metabolism signals, we also described that inhibition of the RAGE pathway after stroke could improve the functional outcome after stroke in mice. RAGE is a multiligand membrane receptor and localizes on all types of cells.[33] The activation of RAGE on neurons had been shown to stimulate the production of reactive oxygen species and lead to death.[34] RAGE also is involved in the recruitment of neutrophils recruited by HMGB1,[35] indicating that neutrophils might mediated the effects attributed to RAGE. In addition, RAGE is also involved in regulating the activation of infiltrating brain macrophages.[22] Therefore, interference with RAGE signaling could improve brain damage in multiple ways after stroke. Our study using *in vivo* or *in vitro* experiments demonstrated that RAGE receptor signaling has a direct role in regulating the transcriptional and metabolic alteration of $CD4^+$ cells after stroke. Surprisingly, our data showed that inhibiting RAGE after stroke did not lead to significantly $CD4^+$ T cell increased after MCAO, which was inconsistent with the previous report by Liesz et al.[19] The discrepancy could be attributed to the differences in the drug administration strategies/timepoint and the degree of disease damage. Meanwhile, inhibiting RAGE increased the proportion of Treg and reduced the generation of Th17 after stroke. Treg/Th17 ratio is an important mechanism of immune regulation of stroke, and its increase in the acute phase of stroke often represents a better prognosis.[14,17,36–38] Therefore, we believe that inhibition of RAGE could reduce the ischemic brain injury and improve function outcome after stroke.

There are also some limitations in this study. First of all, the effect of TLR4 receptor on peripheral $CD4^+$ cells was not discussed in this paper because the expression of TLR4 was changed in spleen but not in blood. In addition, T cell RAGE signaling and IRF7-based interferon signaling pathways were linked together for the first time in this article, but further verification will be important. Secondly, RAGE can be expressed not only on $CD4^+$ T cells, but also on a variety of peripheral immune cells. Therefore, neutralization of RAGE could potentially affect the transcriptional and metabolic profiles of other immune cells. More specific conditional knockout mice are needed to address the role of RAGE on $CD4^+$ T cells in the ischemic brain injury.

In summary, we demonstrate that RAGE signaling regulates the metabolic reprogramming of $CD4^+$ T cells and its differentiation into Th17 and Treg cells after cerebral ischemic injury. In addition, sRAGE treatment reduces ischemic brain infarct and ameliorates functional recovery after stroke by inhibiting fatty acid synthesis, favoring $CD4^+$ T cells polarization toward Treg, which could represent a novel immune-metabolic therapy for the treatment of neuroinflammation after ischemic stroke.

Funding

The author(s) disclosed receipt of the following financial support for the research, authorship, and/or publication of this article: P.L. is supported by the National Natural Science Foundation of China (NSFC, 81722017, 91957111, 81971096, 82061130224), New Frontier Technology Joint Research sponsored by Shanghai Shenkang Hospital Development Center (SHDC12019102), Shanghai Municipal Education Commission-Gaofeng Clinical Medical Grant Support (20181805), Shuguang Program" supported by Shanghai Education Development Foundation and Shanghai Municipal Education Commission (20SG17), and Shanghai Outstanding Academic Leaders' Program from Shanghai Municipal Science and Technology Committee (20XD1422400), Newton Advanced Fellowship grant provided by the UK Academy of Medical Sciences (NAF\R11 \1010), Shanghai Municipal Key Clinical Specialty (shslczdzk03601 to Weifeng Yu), Innovation Program of Shanghai Municipal Education Commission (2019-01-07-00-01-E00074 to Weifeng Yu).

Declaration of conflicting interests

The author(s) declared no potential conflicts of interest with respect to the authorship, and/or publication of this article.

Authors' contributions

YZ, FL, CC and DH performed the experiments. YZ, FL, XZ and YL collected the data and performed the analysis. YZ, PL and WX wrote the manuscript. WY and PL designed the experiments. JW and PL supervised the project.

Supplemental material

Supplemental material for this article is available online.

ORCID iD

Peiying Li https://orcid.org/0000-0002-5721-9914

References

1. Hurford R, Wolters FJ, Li L, et al. Prevalence, predictors, and prognosis of symptomatic intracranial stenosis in patients with transient ischaemic attack or minor stroke: a population-based cohort study. *Lancet Neurol* 2020; 19: 413–421.
2. Man S, Xian Y, Holmes DN, et al. Association between thrombolytic door-to-needle time and 1-year mortality and readmission in patients with acute ischemic stroke. *Jama* 2020; 323: 2170–2184.
3. Park YJ and Borlongan CV. Recent advances in cell therapy for stroke. *J Cereb Blood Flow Metab* 2021; 41: 2797–2799.

4. An C, Shi Y, Li P, et al. Molecular dialogs between the ischemic brain and the peripheral immune system: dualistic roles in injury and repair. *Prog Neurobiol* 2014; 115: 6–24.
5. Na SY, Mracsko E, Liesz A, et al. Amplification of regulatory T cells using a CD28 superagonist reduces brain damage after ischemic stroke in mice. *Stroke* 2015; 46: 212–220.
6. Heindl S, Ricci A, Carofiglio O, et al. Chronic T cell proliferation in brains after stroke could interfere with the efficacy of immunotherapies. *J Exp Med* 2021; 218: e20202411.
7. Li S, Huang Y, Liu Y, et al. Change and predictive ability of circulating immunoregulatory lymphocytes in long-term outcomes of acute ischemic stroke. *J Cereb Blood Flow Metab* 2021; 41: 2280–2294.
8. Huang X, Hussain B and Chang J. Peripheral inflammation and blood-brain barrier disruption: effects and mechanisms. *CNS Neurosci Ther* 2021; 27: 36–47.
9. Liesz A, Suri-Payer E, Veltkamp C, et al. Regulatory T cells are key cerebroprotective immunomodulators in acute experimental stroke. *Nat Med* 2009; 15: 192–199.
10. Li P, Gan Y, Sun BL, et al. Adoptive regulatory T-cell therapy protects against cerebral ischemia. *Ann Neurol* 2013; 74: 458–471.
11. Li P, Mao L, Zhou G, et al. Adoptive regulatory T-cell therapy preserves systemic immune homeostasis after cerebral ischemia. *Stroke* 2013; 44: 3509–3515.
12. Wang HY, Ye JR, Cui LY, et al. Regulatory T cells in ischemic stroke. *Acta Pharmacol Sin* 2021. DOI: 10.1038/s41401-021-00641-4.
13. Wang H, Wang Z, Wu Q, et al. Regulatory T cells in ischemic stroke. *CNS Neurosci Ther* 2021; 27: 643–651. 2021/01/21. DOI: 10.1111/cns.13611.
14. Shi L, Sun Z, Su W, et al. Treg cell-derived osteopontin promotes microglia-mediated white matter repair after ischemic stroke. *Immunity* 2021; 54: 1527–1542.e8.
15. Yang K, Blanco DB, Neale G, et al. Homeostatic control of metabolic and functional fitness of Treg cells by LKB1 signalling. *Nature* 2017; 548: 602–606.
16. Berod L, Friedrich C, Nandan A, et al. De novo fatty acid synthesis controls the fate between regulatory T and T helper 17 cells. *Nat Med* 2014; 20: 1327–1333.
17. Wang X, Zhou Y, Tang D, et al. ACC1 (acetyl coenzyme a carboxylase 1) is a potential immune modulatory target of cerebral ischemic stroke. *Stroke* 2019; 50: 1869–1878.
18. Roth S, Singh V, Tiedt S, et al. Brain-released alarmins and stress response synergize in accelerating atherosclerosis progression after stroke. *Sci Transl Med* 2018; 10: 03–16. 2018//DOI: 10.1126/scitranslmed.aao1313.
19. Liesz A, Dalpke A, Mracsko E, et al. DAMP signaling is a key pathway inducing immune modulation after brain injury. *J Neurosci* 2015; 35: 583–598.
20. Xie J, Mendez JD, Mendez-Valenzuela V, et al. Cellular signalling of the receptor for advanced glycation end products (RAGE). *Cell Signal* 2013; 25: 2185–2197.
21. Li P, Wang L, Zhou Y, et al. C-C chemokine receptor type 5 (CCR5)-mediated docking of transferred tregs protects against early blood-brain barrier disruption after stroke. *Jaha* 2017; 6: e006387.
22. Muhammad S, Barakat W, Stoyanov S, et al. The HMGB1 receptor RAGE mediates ischemic brain damage. *J Neurosci* 2008; 28: 12023–12031.
23. Percie Du Sert N, Hurst V, Ahluwalia A, et al. The ARRIVE guidelines 2.0: updated guidelines for reporting animal research. *J Cereb Blood Flow Metab* 2020; 40: 1769–1777.
24. Cekanaviciute E, Fathali N, Doyle KP, et al. Astrocytic transforming growth factor-beta signaling reduces subacute neuroinflammation after stroke in mice. *Glia* 2014; 62: 1227–1240.
25. Rogers DC, Campbell CA, Stretton JL, et al. Correlation between motor impairment and infarct volume after permanent and transient Middle cerebral artery occlusion in the rat. *Stroke* 1997; 28: 2060–2066.
26. Bouet V, Boulouard M, Toutain J, et al. The adhesive removal test: a sensitive method to assess sensorimotor deficits in mice. *Nat Protoc* 2009; 4: 1560–1564.
27. Varanasi SK, Kumar SV and Rouse BT. Determinants of tissue-specific metabolic adaptation of T cells. *Cell Metab* 2020; 32: 908–919.
28. Chamorro A, Meisel A, Planas AM, et al. The immunology of acute stroke. *Nat Rev Neurol* 2012; 8: 401–410.
29. Wood TR, Vu PT, Comstock BA, et al. Cytokine and chemokine responses to injury and treatment in a nonhuman primate model of hypoxic-ischemic encephalopathy treated with hypothermia and erythropoietin. *J Cereb Blood Flow Metab* 2021; 41: 2054–2066.
30. Li Y, Zhu ZY, Huang TT, et al. The peripheral immune response after stroke-A double edge sword for blood-brain barrier integrity. *CNS Neurosci Ther* 2018; 24: 1115–1128.
31. Brown J, Kingsbury C, Lee JY, et al. Spleen participation in partial MHC class II construct neuroprotection in stroke. *CNS Neurosci Ther* 2020; 26: 663–669.
32. Wong CH, Jenne CN, Lee WY, et al. Functional innervation of hepatic iNKT cells is immunosuppressive following stroke. *Science* 2011; 334: 101–105.
33. Li J, Zeng Q, Su W, et al. FBXO10 prevents chronic unpredictable stress-induced behavioral despair and cognitive impairment through promoting RAGE degradation. *CNS Neurosci Ther* 2021; 27: 1504–1517.
34. Vincent AM, Perrone L, Sullivan KA, et al. Receptor for advanced glycation end products activation injures primary sensory neurons via oxidative stress. *Endocrinology* 2007; 148: 548–558.
35. Orlova VV, Choi EY, Xie C, et al. A novel pathway of HMGB1-mediated inflammatory cell recruitment that requires mac-1-integrin. *Embo J* 2007; 26: 1129–1139.
36. Mao L, Li P, Zhu W, et al. Regulatory T cells ameliorate tissue plasminogen activator-induced brain haemorrhage after stroke. *Brain* 2017; 140: 1914–1931.
37. Zhang H, Xia Y, Ye Q, et al. In vivo expansion of regulatory T cells with IL-2/IL-2 antibody complex protects against transient ischemic stroke. *J Neurosci* 2018; 38: 10168–10179.
38. Ito M, Komai K, Mise-Omata S, et al. Brain regulatory T cells suppress astrogliosis and potentiate neurological recovery. *Nature* 2019; 565: 246–250.